

Supporting Information

Selective Reactivity-Assisted Sacrificial Additive Coating for Surface Passivation of Wide Bandgap Perovskite Solar Cells with Cesium Tetrafluoroborate

Jaehyuk Koh,^{1, ‡} Daehan Kim,² Sang Woo Park,³ Hyungjun Kim,⁴ Ki-Ha Hong,^{3,*} Byungha Shin^{1,*}

¹ Department of Materials Science and Engineering, Korea Advanced Institute of Science and Technology (KAIST), Daejeon 34141, Republic of Korea.

² Department of Chemistry, Northwestern University, Evanston, Illinois 60208, United States

³ Department of Materials Science and Engineering, Hanbat National University, Daejeon 34158, Republic of Korea

⁴ Department of Chemistry, Korea Advanced Institute of Science and Technology (KAIST), Daejeon 34141, Republic of Korea.

* Corresponding author(s). Email: byungha@kaist.ac.kr, kiha.hong@hanbat.ac.kr

Materials and Methods

Materials

Formamidinium iodide (FAI), methylammonium bromide (MABr), phenethylammonium iodide (PEAI), phenethylammonium thiocyanate (PEASCN), and phenethylammonium tetrafluoroborate (PEABF₄) were purchased from Greatcell Solar. Lead iodide (PbI₂), and lead bromide (PbBr₂) were purchased from TCI chemicals. Cesium iodide (CsI), lead thiocyanate (Pb(SCN)₂), dimethylformamide (DMF), N-methyl-2-pyrrolidone (NMP), toluene, isopropyl alcohol (IPA), methanol, and polyethylenimine (PEIE, 80% ethoxylated solution) were purchased from Sigma-Aldrich. Poly(triaryl amine) (PTAA) was purchased from EMNI. Fullerene (C₆₀) was purchased from nano-C. Diethyl ether (DEE) was purchased from Duksan.

Fabrication of wide-bandgap perovskite solar cells

5 mg/ml of PTAA solution (in Tol and NMP mixed solvent system) was spin-coated on the ITO substrate at 6000 rpm and then annealed at 100°C on a hot plate for 10 min. Wide bandgap perovskite solutions were prepared by dissolving FAI, MABr, CsI, PbI₂, PbBr₂, Pb(SCN)₂, PEA, and PEASCN in DMF and NMP mixed solvent system (DMF:NMP = 4:1 volume ratio). This solution was spin-coated on the PTAA film at 3000 rpm for 10 s, and it was immediately immersed in a DEE bath for 30 s. After bathing, the film was annealed at 100°C for 3 min. For SSC treatment, PEABF₄ solution (in IPA) was spin-coated on the perovskite film. 30 nm-thick C₆₀ layer was deposited on the perovskite film using a thermal evaporator, then 0.2 wt% of PEIE solution (in IPA) was spin-coated at 4500 rpm. Finally, 100 nm of Ag electrode was deposited by a thermal evaporator.

Characterization

X-ray diffractometry (XRD) patterns were collected using Rigaku Ultima IV in theta/2-theta mode. Photoluminescence (PL) measurements were taken using the FL920 Time-correlated single photon counting (TCSPC) system from Edinburgh Instruments. The excitation source was a 530 nm-wavelength pulsed laser. Ultraviolet photoelectron spectroscopy (UPS) (Thermo VG Scientific Sigma Probe) measured the energy alignments of the films. The binding energies of UPS spectra were calibrated by an Au reference. The Thermo VG Scientific Sigma Probe was used to acquire high-resolution XPS spectra, which were calibrated with C 1s of adventitious carbon at 284.80 eV.

Device Characterization

Current density-voltage (J-V) curves were collected under a simulated AM 1.5G illumination (100 mW/cm², Oriel Sol3A Class AAA, Newport) using Keithley 2400 source meter unit under ambient conditions. With a standard Si cell (Newport, KG5 window), the AM 1.5G irradiation was calibrated. All J-V characteristics were measured using a metal aperture with an area of 0.0625 cm² to define the active area of the devices. The scan rate is 200 mV/s. External quantum efficiency (EQE) spectra were measured using a quantum-efficiency measurement system (PV Measurement QEX6).

Computational Methods

The Density Functional Theory (DFT) calculations are carried out utilizing the projector-augmented wave (PAW) method as implemented in the Vienna Ab initio Simulation Package (VASP).^{1,2} The core-valence interaction is described by using the projector-augmented wave (PAW) method.⁴ We adopt plane-wave basis expansions with an energy cutoff set at 520 eV, along with the Perdew-Burke-Ernzerhof (PBE) generalized gradient approximation (GGA) for the exchange-correlation function.³ The Grimme's D3 method is employed for dispersion correction.⁵

To account for the random orientations of molecular cations and the tilting of octahedra, we employ $2 \times 2 \times 2$ supercell structures incorporating 8 cubic unit cells as the initial structures for the bulk FAPbI₃ phase. We examined 10 distinct orientations of molecules and halide mixing configurations to identify the structure with minimum energy. The optimization of lattice structures involved relaxing all atomic positions and lattice constants until the residual forces and energy differences fell below 0.01 eV/Å and 10⁻⁶ eV respectively, achieved using a $2 \times 2 \times 2$ G-centered k-point grid mesh. Slab structures are created by incorporating a vacuum layer into the supercell, with the distance between periodic cells set at over 12 Å to nullify interaction through periodic boundary conditions. The bottom half layers of the structure were frozen to obtain the optimized surface structures. The atomic structures are visualized using the VESTA package.⁶

The formation energies (E_f) are determined by subtracting the energies of molecule-free perovskite surfaces and the molecular energies from the total system energy. Therefore, negative formation energy indicates a spontaneous reaction.

Solvent	Toluene	Chloro- benzene	Iso- propanol	Ethanol	Water
Polarity Index	2.4	2.7	3.9	4.0	10.2
Soluble?	X	X	X	X	△

Table S1. The polarity characteristics of solvents and their ability to dissolve CsBF₄.

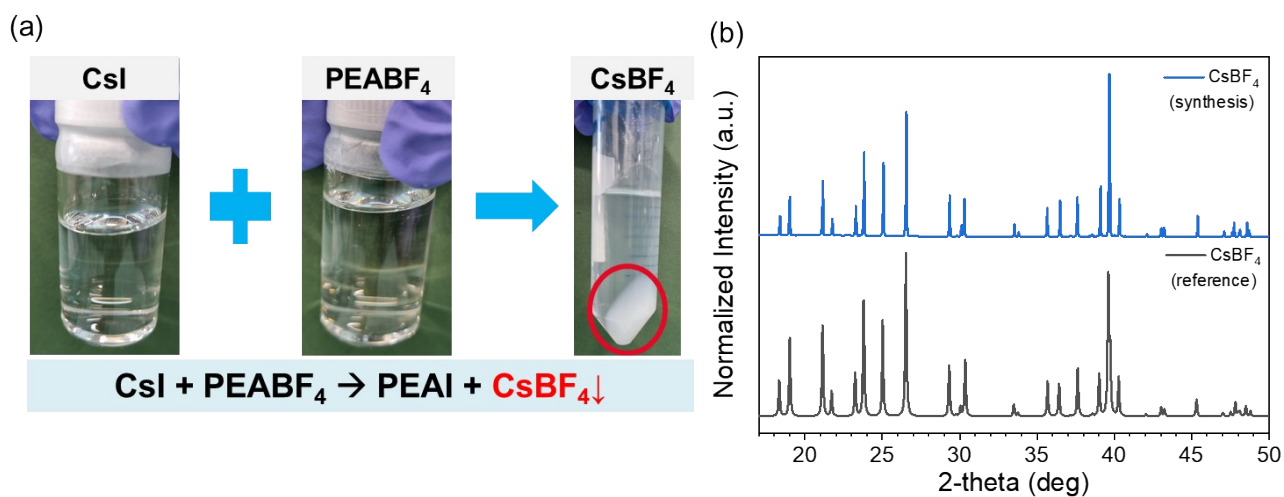


Figure S1. (a) Precipitation reaction between CsI and PEABF₄ in aqueous solution. (b) XRD spectra of the precipitate formed in (a)

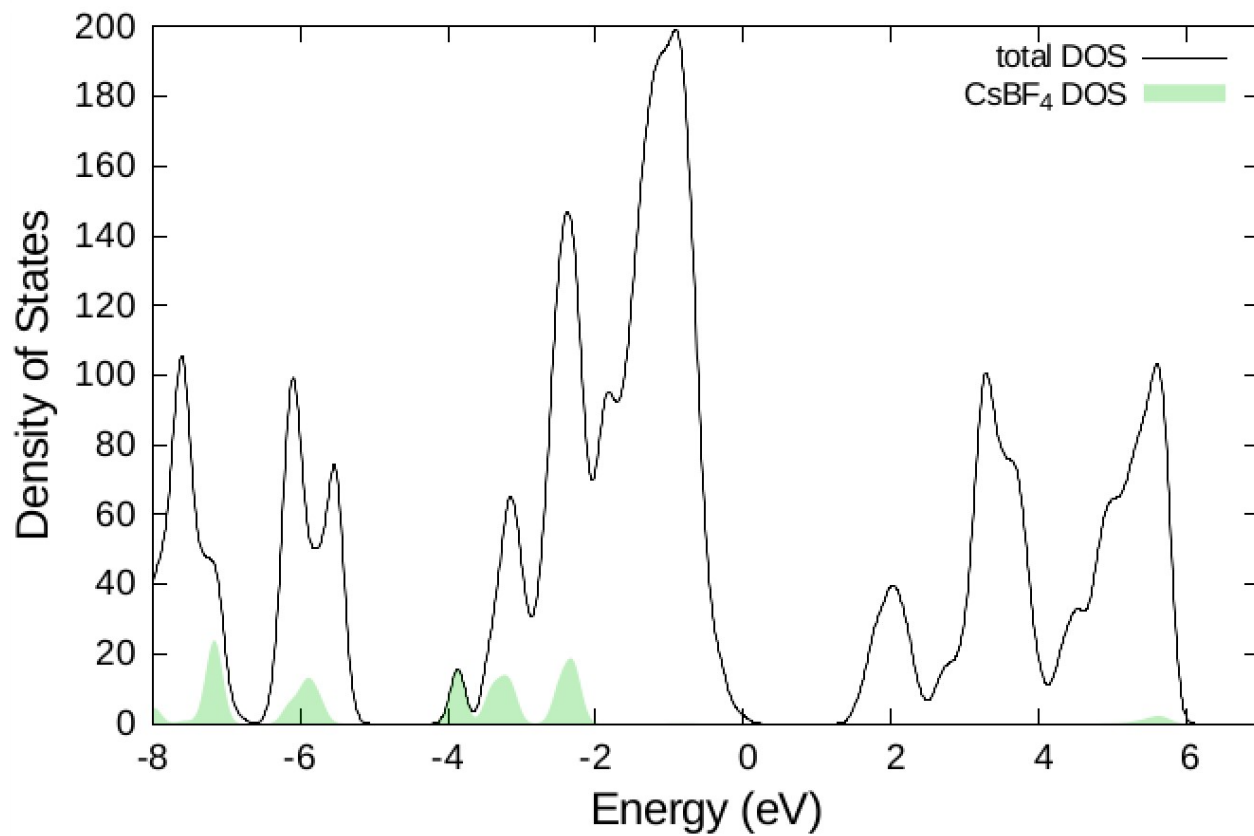


Figure S2 Projected density of states (PDOS) of CsBF₄-passivated FAPbI₃ surface. The valence band maximum is set to 0 eV.

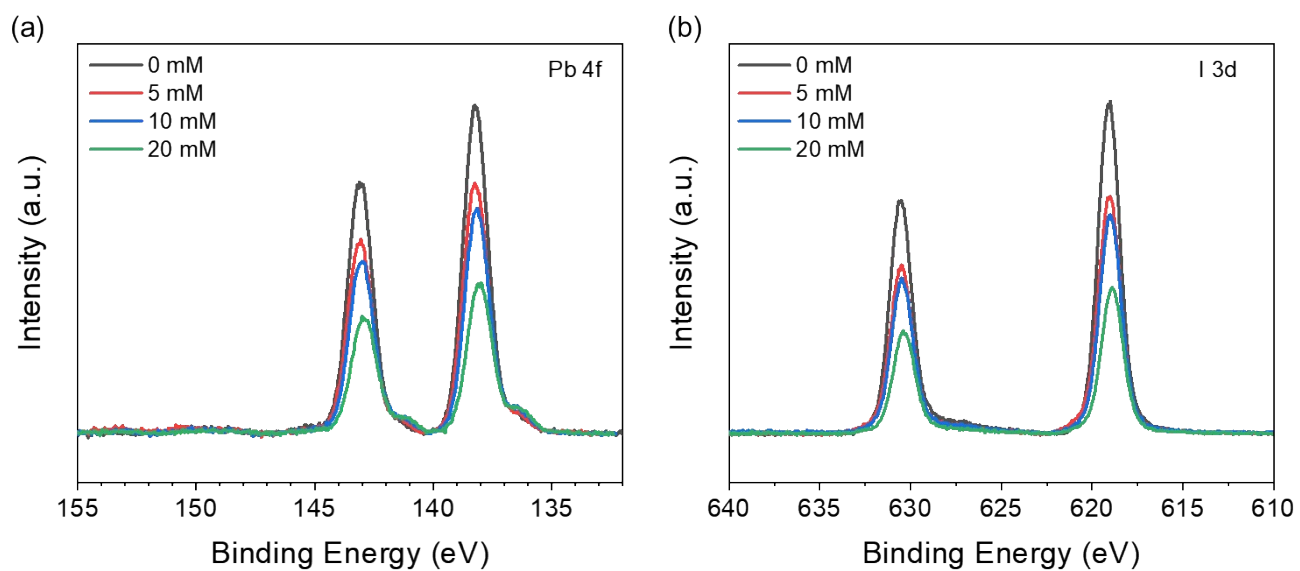


Figure S3. High-resolution (a) Pb 4f and (b) I 3d XPS spectra of perovskite films treated with varying concentrations of PEABF₄ solution.

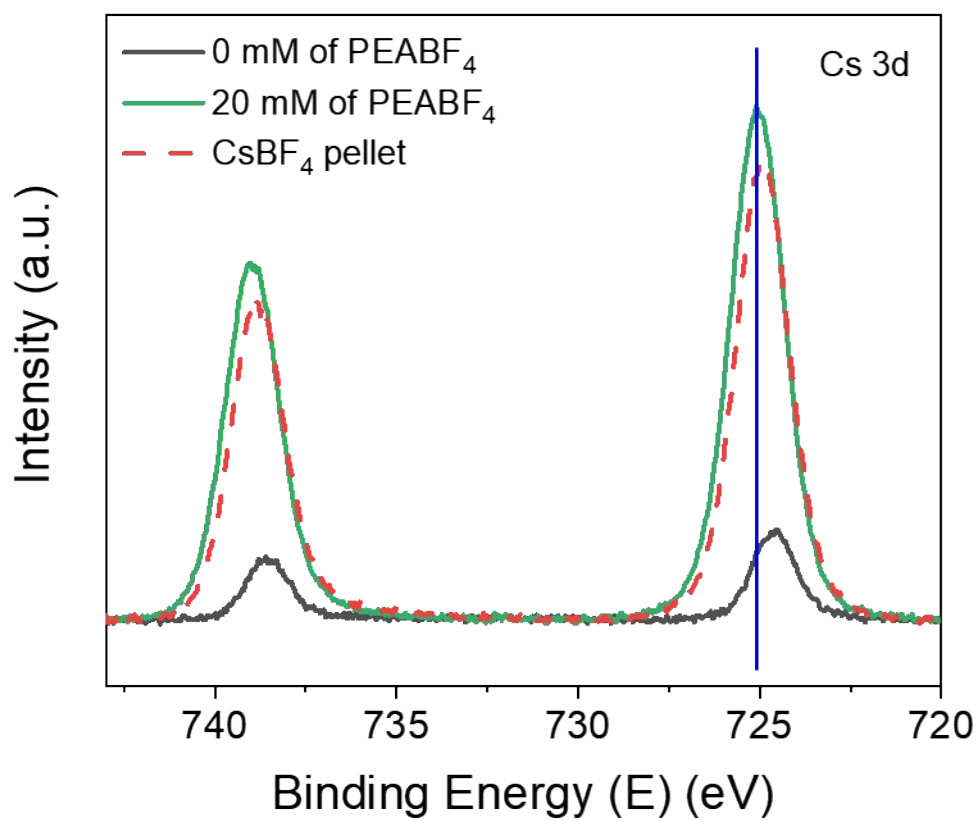


Figure S4. High-resolution Cs 3d XPS spectra of the perovskite film with and without PEABF₄ treatment, and CsBF₄ pellet synthesized in Figure S1.

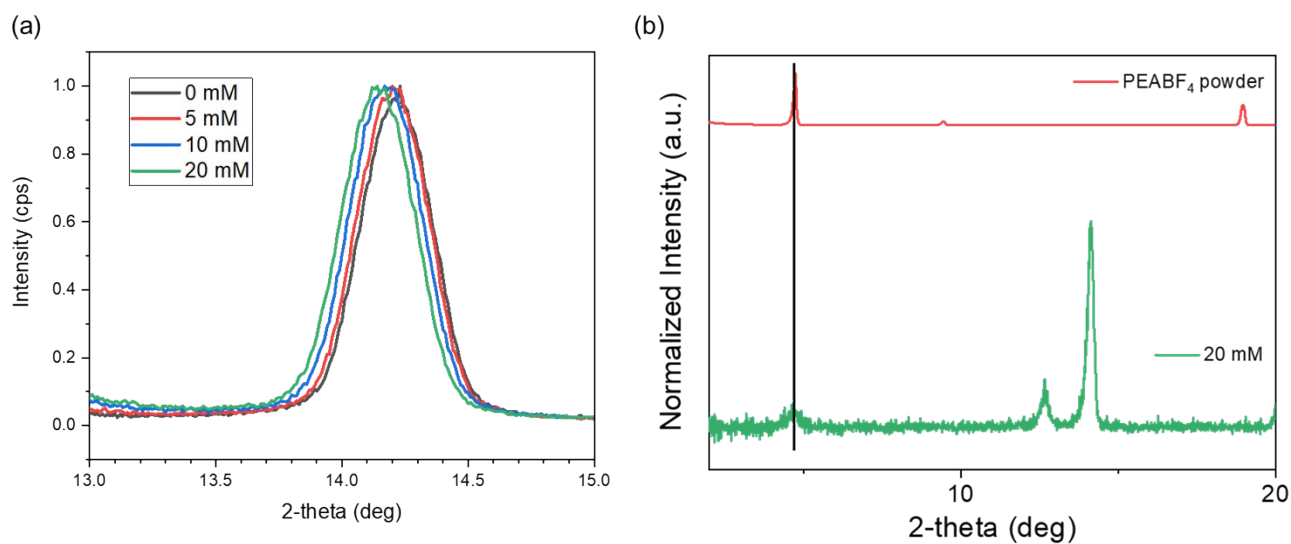


Figure S5. (a) Enlarged version of perovskite peaks of GIXRD spectra in Fig. 2d. (b) XRD patterns of PEABF₄ powder and SSC-treated perovskite film with 20 mM of PEABF₄ solution.

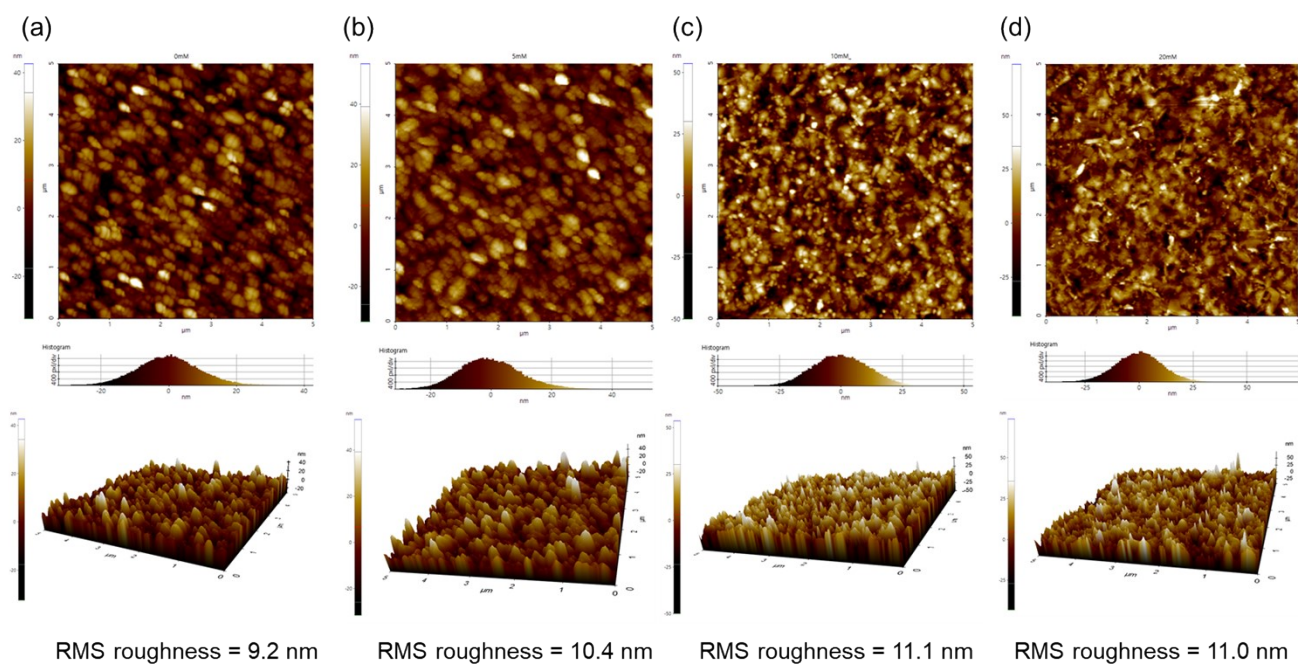


Figure S6. AFM images and rms roughness of the (a) SSC untreated perovskite film and SSC treated perovskite film with (b) 5 mM, (c) 10 mM, (d) 20 mM of PEABF₄ solution.

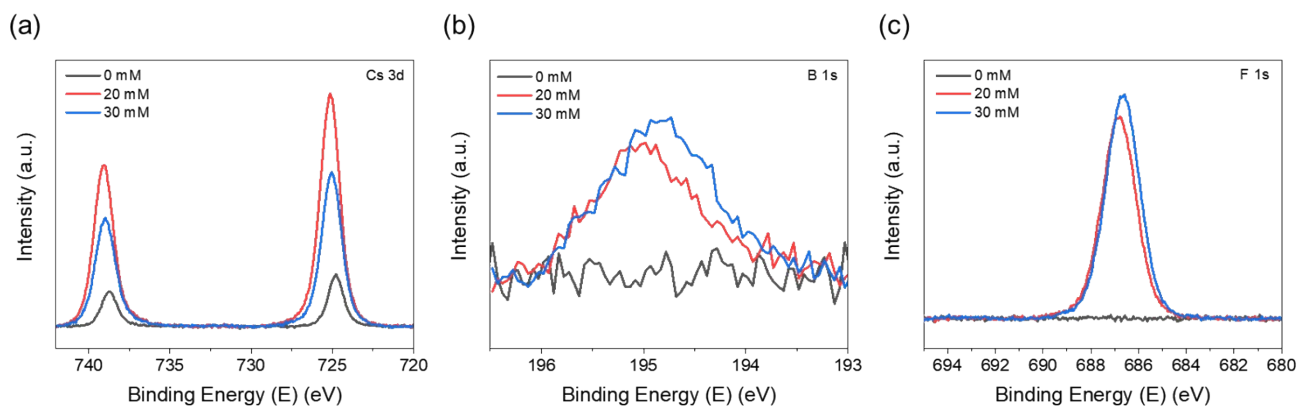


Figure S7. High resolution (a) Cs 3d, (b) B 1s, (c) F 1s XPS spectra of perovskite films treated with higher concentrations of PEABF₄ solution.

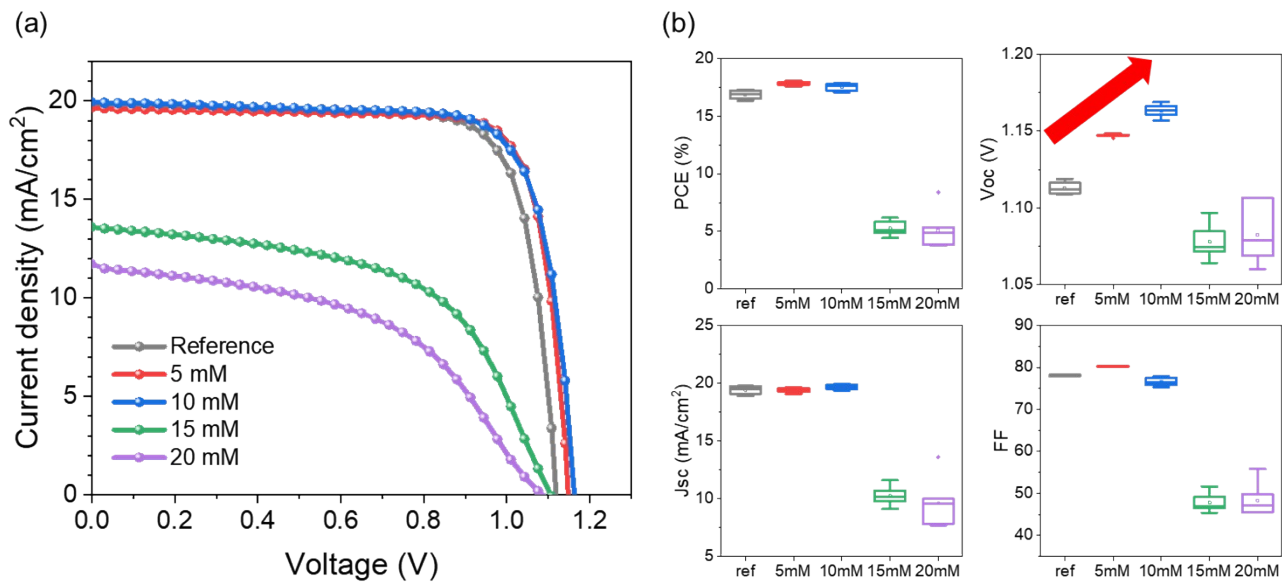


Figure S8. (a) J-V curves and (b) performance parameters of the WBG perovskite solar cells treated with varying concentrations of PEABF₄ solution.

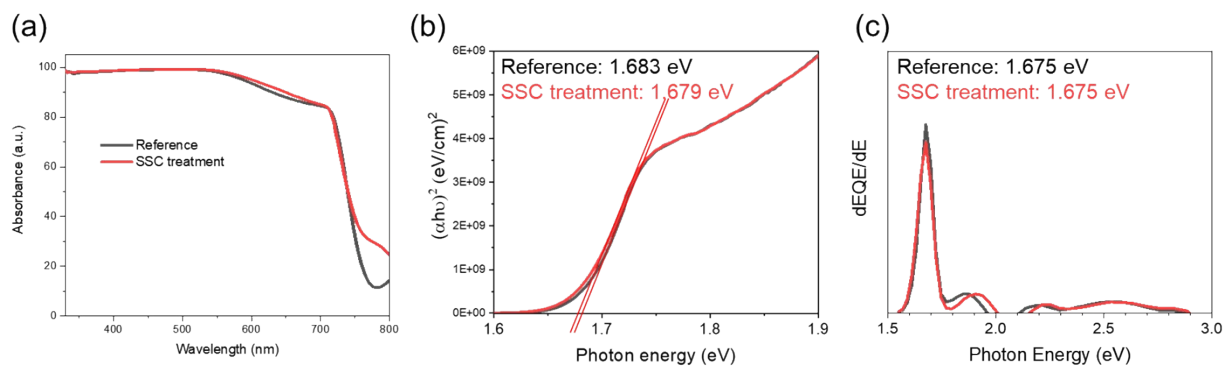


Figure S9. (a) Absorbance spectra, (b) Tauc plot and (C) 1st derivative of EQE spectra of the perovskite films with and without the SSC treatment.

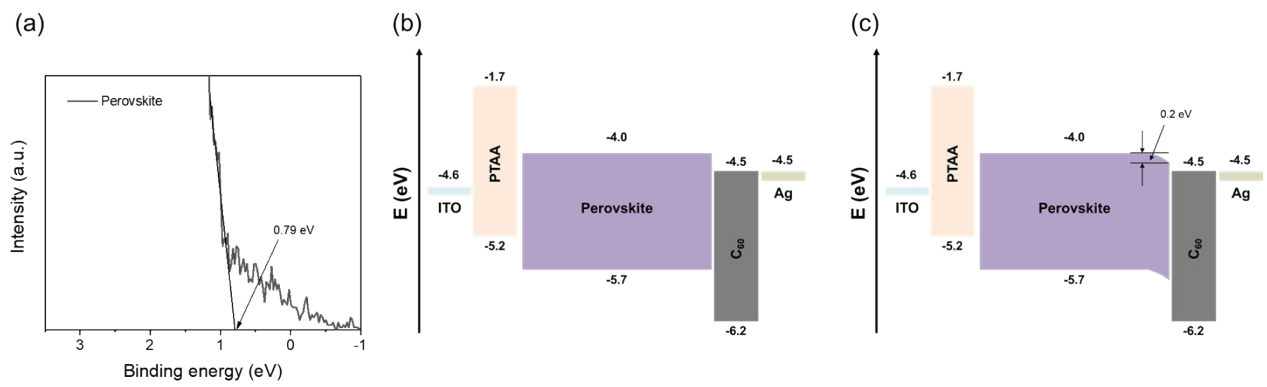


Figure 10. (a) Lower energy cutoff of perovskite film without the SSC treatment. The energy diagram of the devices (b) without and (c) with the SSC treatment. The energy band information of the other functional layers is obtained from other literatures^{7,8}.

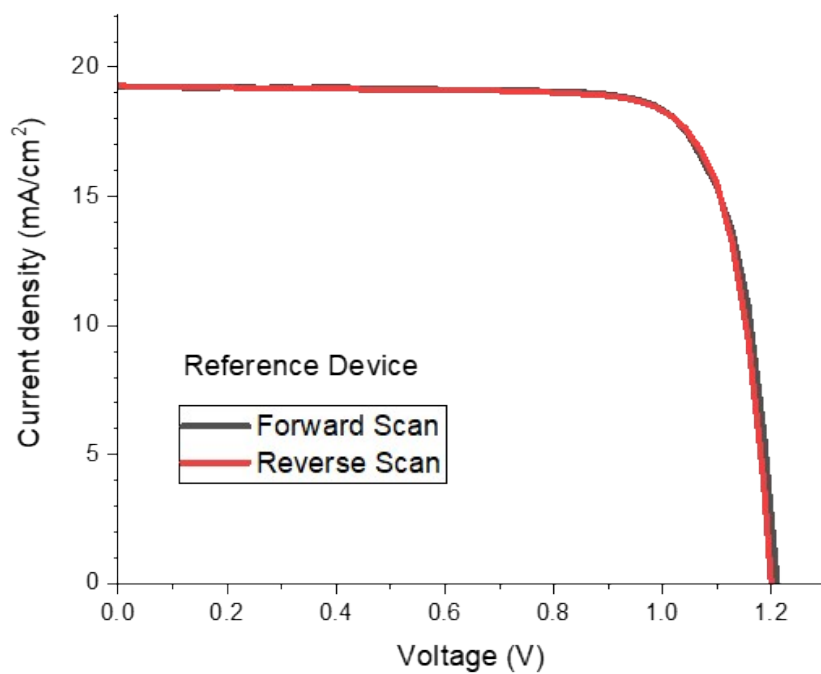
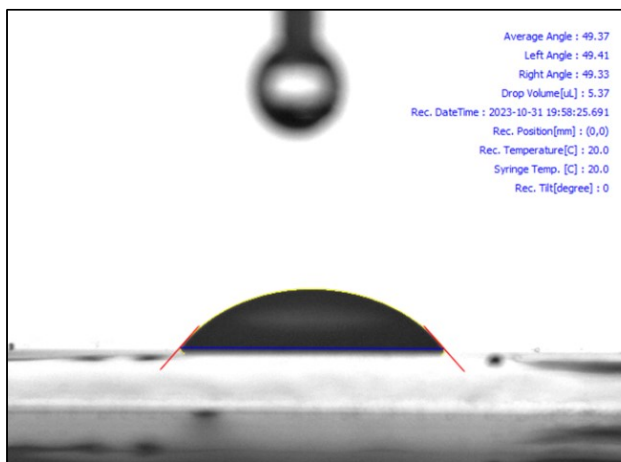


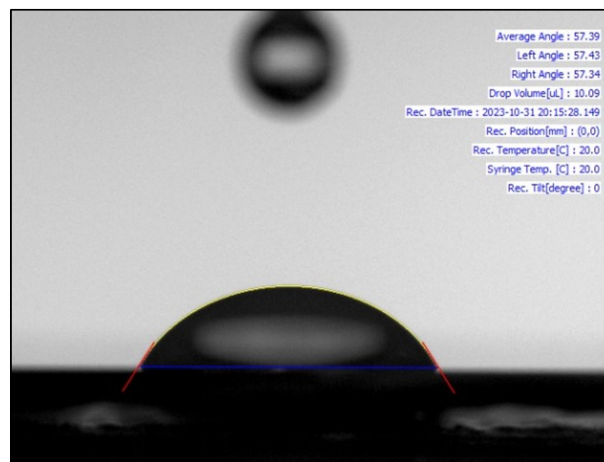
Figure S11. J-V curves of the reference device with forward and reverse scan.

(a)



Contact angle: 49.37°

(b)



Contact angle: 57.39°

Figure S12. Contact angle of water of the perovskite films (a) without and (b) with SSC treatment.

Reference

- (1) Kresse, G.; Hafner, J. Ab Initio Molecular Dynamics for Liquid Metals. *Phys Rev B* 1993, 47 (1), 558–561. <https://doi.org/10.1103/physrevb.47.558>.
- (2) Kresse, G.; Furthmüller, J. Efficiency of Ab-Initio Total Energy Calculations for Metals and Semiconductors Using a Plane-Wave Basis Set. *Comp Mater Sci* 1996, 6 (1), 15–50. [https://doi.org/10.1016/0927-0256\(96\)00008-0](https://doi.org/10.1016/0927-0256(96)00008-0).
- (3) Perdew, J. P.; Burke, K.; Ernzerhof, M. Generalized Gradient Approximation Made Simple. *Phys Rev Lett* 1996, 77 (18), 3865–3868. <https://doi.org/10.1103/physrevlett.77.3865>.
- (4) Blöchl, P. E. Projector Augmented-Wave Method. *Phys Rev B* 1994, 50 (24), 17953–17979. <https://doi.org/10.1103/physrevb.50.17953>.
- (5) Grimme, S.; Antony, J.; Ehrlich, S.; Krieg, H. A Consistent and Accurate Ab Initio Parametrization of Density Functional Dispersion Correction (DFT-D) for the 94 Elements H-Pu. *J Chem Phys* 2010, 132 (15), 154104. <https://doi.org/10.1063/1.3382344>.
- (6) Momma, K.; Izumi, F. VESTA 3 for Three-Dimensional Visualization of Crystal, Volumetric and Morphology Data. *J Appl Crystallogr* 2011, 44 (6), 1272–1276. <https://doi.org/10.1107/s0021889811038970>.
- (7) Khadka, D. B.; Shirai, Y.; Yanagida, M.; Ryan, J. W.; Miyano, K. Exploring the effects of interfacial carrier transport layers on device performance and optoelectronic properties of planar perovskite solar cells. *J. Mater. Chem. C* 2017, 5, 8819. <https://doi.org/10.1039/c7tc02822a>.
- (8) Yin, Y.; Wang, M.; Malgras, V.; Yamauchi, Y. Stable and Efficient Tin-Based Perovskite Solar Cell via Semiconducting-Insulating Structure. *ACS Appl. Energy Mater.* 2020, 3 (11), 10447-10452. <https://doi.org/10.1021/acsaem.0c01422>.